

Simulation of Magnetic Nanoparticle Hyperthermia in Prostate
Tumors

by

Jianan Wang

A thesis submitted to Johns Hopkins University in conformity with the
requirements for the degree of Master of Mechanical Engineering

Baltimore, Maryland

May, 2014

© 2014 Jianan Wang

All Rights Reserved

Abstract

In clinical studies, it is difficult to determine the temperature distribution throughout both tumor and normal tissue during hyperthermia treatment, since temperatures are sampled at only a limited number of locations with conventional sensors. Simulation studies can help physicians understand better the effects of the treatment. In this study, three 2D tumor models are built in the COMSOL software environment based on the images of nanoparticle distributions in sliced PC3, DU145 and LAPC4 tumors. The images are pre-processed in MATLAB before being imported into COMSOL. A uniform distribution model is added as a control group. Temperature distribution, maximum temperature, time to reach steady state, CEM43, iso-effective dose and heat flux at tumor-tissue boundary are analyzed to evaluate the effect of the nanoparticle distribution on hyperthermia treatment. The results indicate that a more concentrated nanoparticle distribution is better in damaging diseased tissue than the uniform distribution under low heating power. A more uniform distribution is better than the concentrated distribution under high heating power. For concentrated nanoparticle distributions, the location where the nanoparticles are concentrated influences tissue damage: a more centered one has a better effect.

Advisor:

Dr. Cila Herman

Department of Mechanical Engineering

Johns Hopkins University

Baltimore, Maryland

Reader:

Dr. Robert Ivkov

Department of Radiation Oncology

Johns Hopkins University School of Medicine

Baltimore, Maryland

Acknowledgments

I would like to express my sincere gratitude to my advisor Prof. Cila Herman for her patient guidance, enthusiastic encouragement and continuous support of my study and research.

Special thank should be given to Dr. Robert Ivkov and Dr. Anilchandra Attaluri, for their professional guidance, valuable support and the offer of images of nanoparticle distributions in sliced prostate tumors.

I would also like to thank Sri Kamal Kandala, my colleague in the research group, for his kind help and stimulating discussions.

Finally, I wish to thank my parents for their support and encouragement throughout my study.

Table of Contents

1. Introduction	1
1.1 Magnetic nanoparticle hyperthermia	1
1.2 Literature review.....	4
1.3 Study goals.....	5
2. Model description	6
2.1 Image generation.....	6
2.2 MATLAB processing.....	7
2.3 COMSOL model.....	10
2.3.1 Geometry and distribution	10
2.3.2 Properties	11
2.3.3 Governing equations.....	13
2.3.4 Boundary and initial conditions.....	15
2.3.5 Time and mesh configuration	16
3. Results and discussion	19
3.1 Temperature distribution.....	19
3.2 Maximum temperature and time to reach steady state	20
3.3 CEM43 contour.....	23
3.4 Iso-effective dose	27
3.5 Heat flux at tumor-tissue boundary	28
3.6 The concentrated model.....	30
4. Conclusions	35

Bibliography	36
Curriculum Vitae	38

List of Tables

Table 1 Properties of tumor and tissue [13-15]	12
Table 2 Thermophysical properties of blood [14, 15]	12
Table 3 Maximum temperature among four models for different mesh types	18
Table 4 Maximum temperature among four models as a function of time steps	18

List of Figures

Figure 1 Magnetic hysteresis	3
Figure 2 Nanoparticle distributions for the tumors (a) PC3 (b) DU145 (c) LAPC4 (Courtesy of Anilchandra Attaluri, Robert Ivkov lab) .	6
Figure 3 Flow chart of MATLAB processing.....	7
Figure 4 Coordinates in MATLAB and in COMSOL	8
Figure 5 (a) Stained pixels in the initial images and (b) stained pixels in MATLAB processed images.....	9
Figure 6 (a) Schematic of the investigated geometry (b) Computational model of PC3, DU145 and LAPC4 tumors with nanoparticles	10
Figure 7 Computational model of the uniform distribution in (a) full view and (b) zoom-in view	11
Figure 8 Flow chart of each time step	15
Figure 9 Meshes of the four models in COMSOL	17
Figure 10 Temperature distribution in tumor and healthy tissue after heating of 1200s for $Q_e=5.51 \times 10^5 \text{W/m}^2$	20
Figure 11 Maximum temperatures in tumor and healthy tissue with time	21
Figure 12 Maximum temperature attained and time needed to reach steady state in (a) tumor and (b) healthy tissue for $Q_e = 5.51 \times 10^5$ W/m^2	21

Figure 13 temperature profiles in different hyperthermia processes [17]	24
.....	24
Figure 14 CEM43=30, 60, 90min for $Q_e = 5.51 \times 10^5 \text{ W/m}^2$	24
Figure 15 Percentage area of (a) tumor and (b) healthy tissue with	
CEM 43> 30, 60, 90min for $Q_e = 5.51 \times 10^5 \text{ W/m}^2$	25
Figure 16 Iso-effective doses for each of the tumor models	27
Figure 17 Heat flux at the tumor–tissue interface for $Q_e = 5.51 \times 10^5$	
W/m^2	28
Figure 18 Computational model of the concentrated model with	
nanoparticles	30
Figure 19 Temperature distributions in tumor and tissue after heating	
of 1200s for $Q_e = 5.51 \times 10^5 \text{ W/m}^2$	30
Figure 20 Maximum temperatures in tumor and healthy tissue with	
time	31
Figure 21 Maximum temperature and time attained at steady state in	
(a) tumor and (b) healthy tissue for $Q_e = 5.51 \times 10^5 \text{ W/m}^2$	31
Figure 22 CEM43=30, 60, 90min for $Q_e = 5.51 \times 10^5 \text{ W/m}^2$	32
Figure 23 Percentage area of (a) tumor and (b) tissue with CEM 43>	
30, 60, 90min for $Q_e = 5.51 \times 10^5 \text{ W/m}^2$	32
Figure 24 Iso-effective doses for each of the tumor models	33
Figure 25 Heat flux at the tumor–tissue interface for $Q_e = 5.51 \times 10^5$	
W/m^2	33

1. Introduction

1.1 Magnetic nanoparticle hyperthermia

Hyperthermia therapy refers to body temperatures elevated to damage cancer cells. It is always used with other forms of cancer therapy, such as radiation therapy and chemotherapy [1]. In hyperthermia, different types of energy may be used to apply heat, including microwave, laser, ultrasound and magnetic fields [2]. Hyperthermia treatments can effectively heat tumors. However, healthy tissues can also absorb microwave, laser and ultrasound energy causing undesired damage. Magnetic nanoparticle hyperthermia uses magnetic field to generate heat. It mainly utilizes EPR effect and magnetic hysteresis to realize hyperthermia. The nanoparticles are spread in tumor tissues and are heated by the external magnetic field. Since the sizes of nanoparticles are smaller than or comparable to those of cells, it is easier for nanoparticles to get close to the targets. Thus, magnetic nanoparticle hyperthermia has the advantage of high efficiency and selective damage.

EPR effect is enhanced permeability and retention effect [3]. Due to higher growth rates in tumor tissue than in normal tissue, tumor cells must stimulate the production of blood vessels to get sufficient nutritional and oxygen supply. The newly formed tumor vessels are usually abnormal in form and architecture. Furthermore, the lymph drainage in

tumor tissue is more likely to be defective. All these factors lead to abnormal molecular and fluid transport dynamics. The injected nanoparticles tend to accumulate in tumor tissue much more than in normal tissue. The EPR effect ensures the injected nanoparticles to be targeted to tumor tissue.

The mechanism of magnetic heating is called magnetic hysteresis [4]. Ferromagnetic materials have atomic dipoles that have both magnitude and direction. When an external magnetic field is applied to a ferromagnetic material, the atomic dipoles are forced to align with the external field, thus being magnetized. If the magnetic field is alternating at a certain frequency, the magnitude and direction of the magnetization would vary periodically. Fig.1 shows the relation of the magnetization and the magnetic field in a ferromagnetic material.

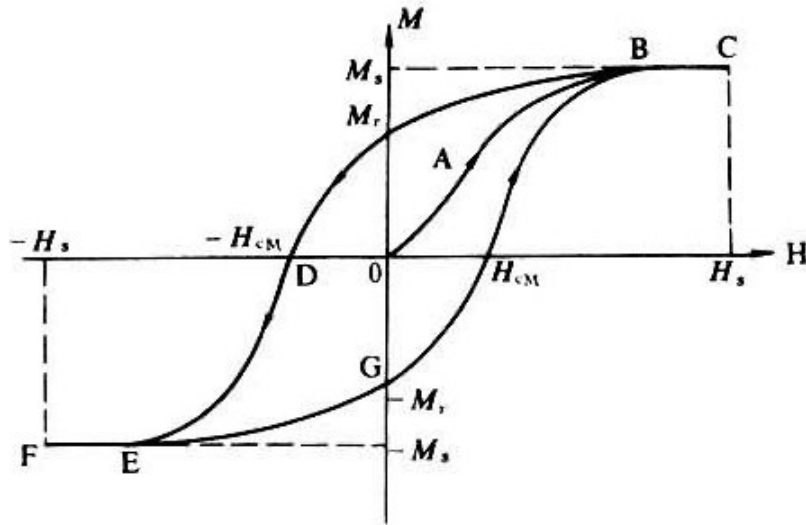


Figure 1 Magnetic hysteresis

In fig.1, it can be observed that the material starts to be magnetized at the magnitude of external magnetic field H_{cM} . As the magnitude of the external field (H) increases, the magnitude of the induced magnetic field in the material (M) is also increased. If H reaches H_s , the material is totally magnetized and M becomes M_s . When the direction of H starts to change to the opposite at point B, the magnitude of M decreases. There is a phase lag between M and H , so when H is zero, M has value of M_r . The material is demagnetized ($M=0$) when H is $-H_{cM}$.

In hysteresis process energy is irreversibly lost. The lost energy is finally transferred to heat. The power of energy lost is calculated as:

$$P = \mu_0 f \oint M dH \quad (1)$$

where μ_0 , f , M , H is the vacuum magnetic permeability, the field frequency, the magnetization and the magnetic field, respectively [4].

1.2 Literature review

Gilchrist et al. [5] first proposed the magnetic materials in hyperthermia in 1957. Hergt et al. [6] confirmed the feasibility of commercially available magnetic iron oxide particles in hyperthermia treatment by conducting *in vitro* experiments. Moroz et al. [7] proved the targeting feature of ferromagnetic particles in liver tumors. With the development of nanotechnology and methods of synthesizing magnetic nanoparticles, magnetic nanoparticle hyperthermia has received increasing attention recently.

Simulation studies of magnetic hyperthermia have been conducted since 1980s. One of the difficulties in clinical hyperthermia studies is the determination of the complete temperature field in both tumors and healthy tissues since temperatures are measured at only a limited number of points when discrete sensors are used [8]. It is therefore difficult to evaluate the efficiency of treatment protocols. Simulation studies of hyperthermia have the advantages of low cost, convenience and accuracy. More importantly, simulations can provide researchers with detailed information regarding the temperature field as well as other clinical parameters in tumors and healthy tissue.

Simulations of magnetic nanoparticle hyperthermia have been conducted since 1980s. Halac et al. [9] analyzed a 1D inhomogeneous model of the abdominal and pelvic regions subjected to a uniform power deposition. Matloubieh et al. [10] built a 2D steady state model with uniformly distributed ferromagnetic seed implants and calculated the temperature distributions. Zhao et al. [11] built a spherical model based on experimental studies on head and neck cancer. In the model, the fluid with ferromagnetic nanoparticles is assumed to be uniformly distributed in the porous tissue.

1.3 Study goals

Most of the simulation studies consider uniform nanoparticle distribution and a uniform power field, which is not realistic. Few simulations have been carried out using realistic nanoparticle distributions. Our work uses three types of real distributions based on the clinical results for prostate cancer. The study is aimed at providing physicians with more realistic simulation results as well as guidance in selecting appropriate treatment parameters for magnetic nanoparticle hyperthermia.

2. Model description

2.1 Image generation

In the previous clinical study, three types of commonly used human prostate xenograft tumors (PC3, DU145 and LAPC4) were obtained by inoculating corresponding tumor cells in mice. Once the tumor has reached the size of $0.15 \pm 0.02 \text{ cm}^3$, intratumoral injections of the aqueous formulation of starch-coated magnetic iron oxide nanoparticle (MION, BNF-starch, 100 nm) were performed to achieve the iron concentration of 5.5mg Fe/cc in the tumor. Twenty-four hours after the injections, tumors were harvested from the mice and were stained with Prussian blue. Then the tumors were sliced and imaged to obtain the nanoparticle distributions. Fig.2 shows the nanoparticle distributions of the three tumors (Courtesy of Anilchandra Attaluri, Robert Ivkov lab).

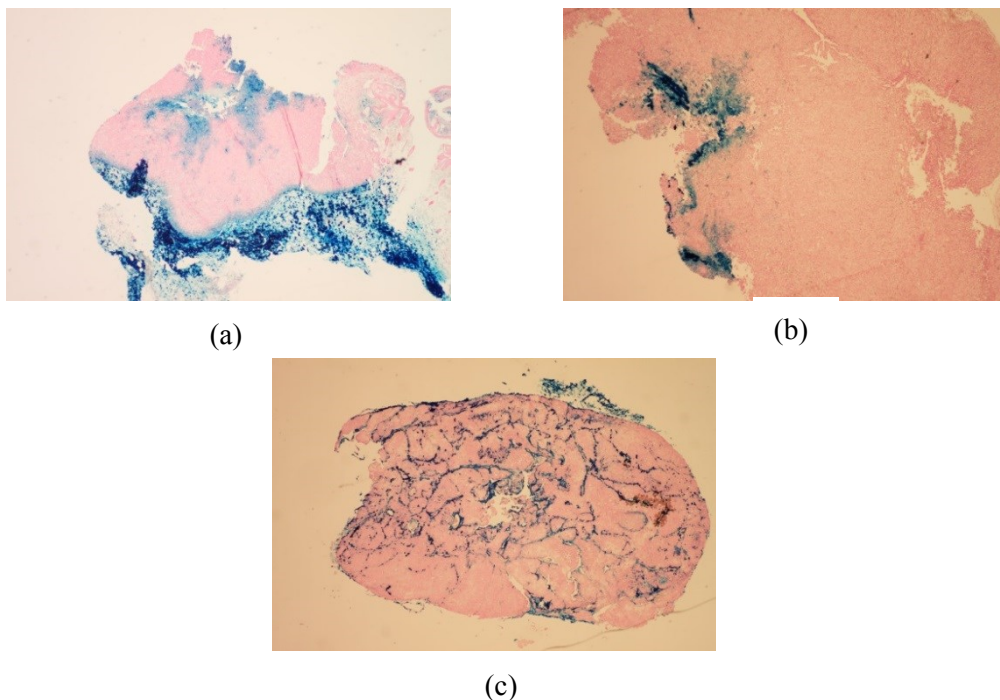


Figure 2 Nanoparticle distributions for the tumors (a) PC3 (b) DU145 (c) LAPC4 (Courtesy of Anilchandra Attaluri, Robert Ivkov lab)

2.2 MATLAB processing

The images shown in fig.2 are processed in MATLAB prior to being imported into COMSOL models. Fig.3 shows the procedures in MATLAB processing.

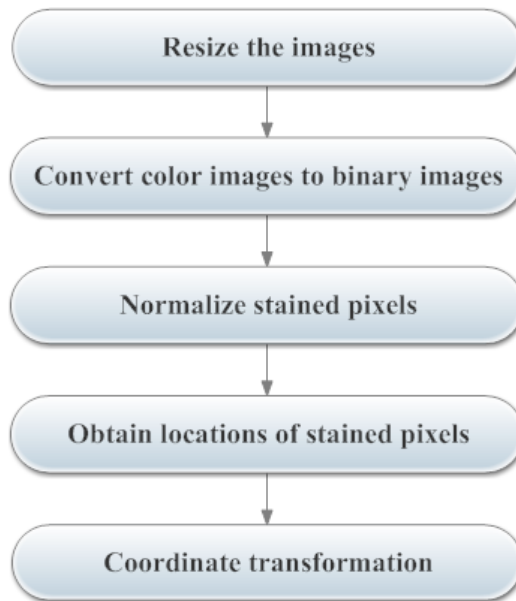


Figure 3 Flow chart of MATLAB processing

First, the obtained high-resolution color images (4752×3168) are resized to smaller color images (225×150) to make the COMSOL models affordable in terms of computational effort. The percentage of stained pixels in the initial image is 10.0% while that of stained pixels in the resized image is 8.5%. Thus, the information regarding nanoparticle distribution in the images is conserved with a reasonable loss, no greater than 1.5%.

Next, the resized color images are converted into binary images. This step

is to distinguish nanoparticles from the tumor tissues in the images so that the location of nanoparticles can be recognized in MATLAB. In the converting process, the number of stained pixels is determined by the value of threshold. If the value of intensity at one pixel is below the threshold, the pixel is recognized as a stained pixel, otherwise it is not. To make the models comparable, the numbers of stained pixels are all normalized to 1460 in the three models by adjusting their thresholds. Next the locations of stained pixels are obtained and stored in the MATLAB mat file. Since the coordinates in MATLAB and those in COMSOL are different (fig.4), a coordinate transformation is performed to make the processed images ready to be imported into COMSOL. Fig.5 compares the nanoparticle distributions in the initial images (fig.5a) and in the processed images (fig.5b).

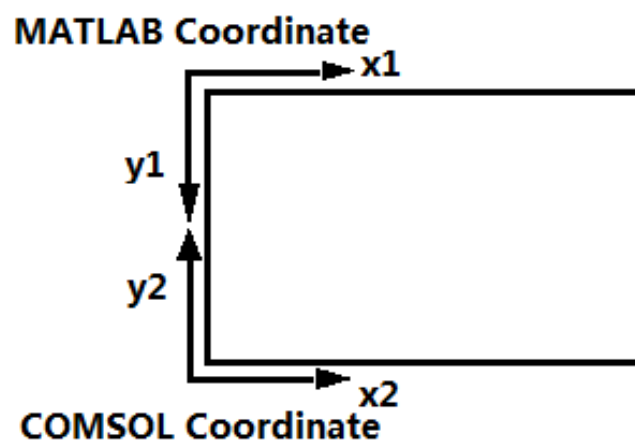


Figure 4 Coordinates in MATLAB and in COMSOL

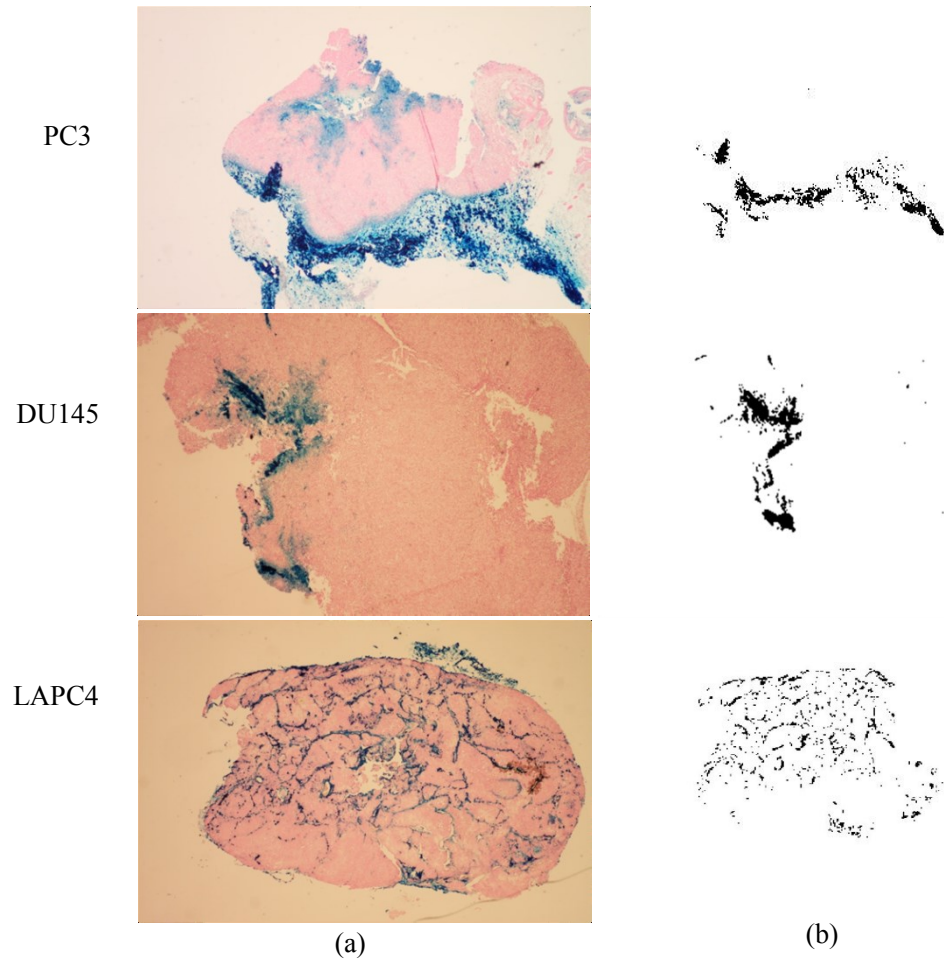


Figure 5 (a) Stained pixels in the initial images and (b) stained pixels in MATLAB processed images

2.3 COMSOL model

2.3.1 Geometry and distribution

COMSOL Multiphysics 4.3 is used to build geometrical and thermal models. A 2D model is built by assuming an elliptic tumor and an elliptic-shaped healthy tissue surrounding the tumor (fig.6a). The nanoparticle distributions obtained from the processed images (fig.5b) were mapped into the tumors (fig.6b). The three nanoparticle

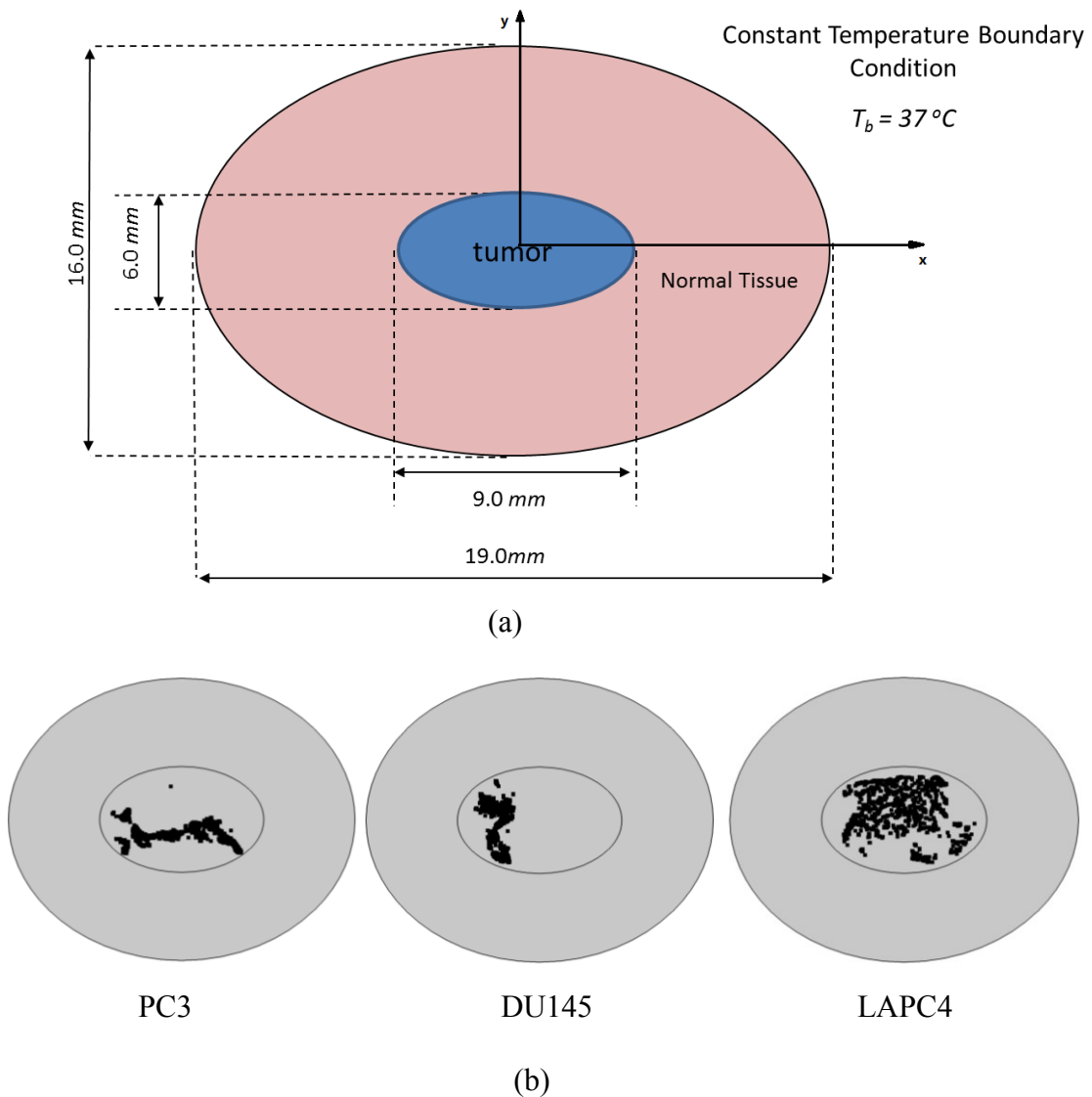


Figure 6 (a) Schematic of the investigated geometry (b) Computational model of PC3, DU145 and LAPC4 tumors with nanoparticles

distributions will yield three thermal models. In addition to the three nanoparticle distributions obtained from tumor slices, we also consider one control model which has a uniform distribution of nanoparticles (fig.7). The spacing is $\Delta x = 1.5\Delta y$, where Δx and Δy are discrete unit in horizontal and vertical directions. The results from the control model are considered as standard results because uniform distribution is thought to be the ideal condition. We use these results to determine parameter values and compare with results from other models. The four models are denoted as PC3, DU145, LAPC4 and Uniform.

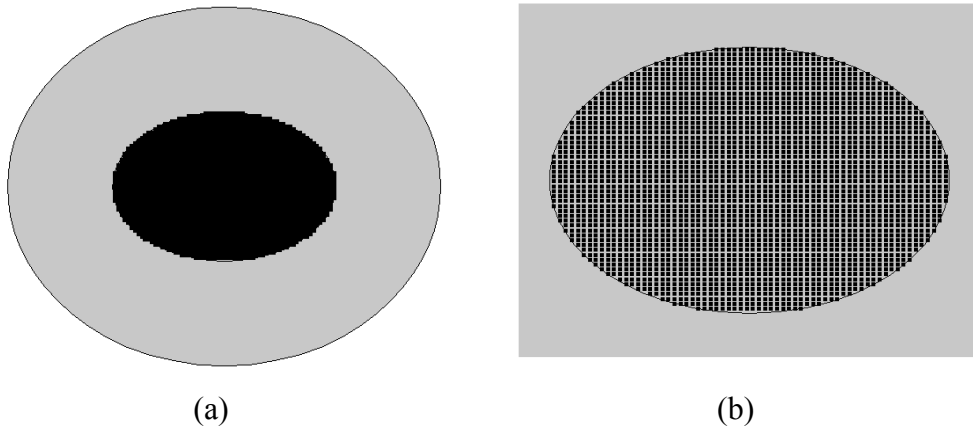


Figure 7 Computational model of the uniform distribution in (a) full view and (b) zoom-in view

2.3.2 Properties

The thermophysical and other properties of the tumor and healthy tissue are summarized in Table 1 [13-15]. The properties of blood are summarized in Table 2 [14, 15]. We assume same properties for each of

the four models since the study focuses on the influence of different nanoparticle distributions on the hyperthermia treatment.

<i>Layer</i>	<i>Pre-factor A(1/s)</i>	<i>Activation Energy E_a(J/mol)</i>	<i>Point heat source Q_p (W/m)</i>	<i>Initial Perfusion Rate ω(1/s)</i>	<i>Metabolic heat rate Q_m (W/m³)</i>
<i>Tumor</i>	1.80 x 10 ³⁶	2.38 x 10 ⁵	0.016	0.0095	31872.5
<i>Healthy Tissue</i>	1.03 x 10 ³⁸	2.49 x 10 ⁵	0	0.003	6374.5

<i>Layer</i>	<i>Specific heat c(J/kg.K)</i>	<i>Density ρ(kg/m³)</i>	<i>Thermal conductivity k (W/m.K)</i>
<i>Tumor</i>	3760	1045	0.51
<i>Healthy Tissue</i>	3760	1045	0.51

Table 1 Properties of tumor and tissue [13-15]

<i>Layer</i>	<i>Specific heat c_b(J/kg.K)</i>	<i>Density ρ_b(kg/m³)</i>	<i>Temperature T_b(°C)</i>
<i>Blood</i>	3770	1060	37

Table 2 Thermophysical properties of blood [14, 15]

The point heat source (Q_p) in Table 1 is chosen as 0.016 W/m so that the maximum temperature in the control model (uniform distribution model) does not exceed 46°C, which is a common maximum temperature in clinical studies [16]. The specific heat loss (SPL, W/g) related to Q_p can

be calculated as:

$$SPL = \frac{Q_p \times N}{C_{Fe} A_t} \quad (2)$$

where N , C_{Fe} , A_t are the number of stained pixels, iron concentration in tumor and area of tumor, respectively.

Once the SPL is determined, the corresponding magnetic field can be calculated by interpolating the data from the relation table in [19]. When Q_p is 0.016W/m, the magnetic field is 29kA/m.

The heat source can also be expressed as Q_e the average heat power per unit tumor area.

$$Q_e = \frac{Q_p \times N}{A_t} \quad (3)$$

where N denotes the number of stained pixels and A_t the area of the tumor.

When Q_p is 0.016 W/m, Q_e is 5.51×10^5 W/m². For convenience, we will use the Q_e to describe heat sources in the paper.

2.3.3 Governing equations

The governing equation describing the heat transfer in the tumor and in

the healthy tissue is the modified Pennes' bio heat equation that also accounts for the thermal damage to tissue [12] as:

Tumor:

$$\rho_t c_t \frac{\partial T_t(x, y, t)}{\partial t} = k_t \nabla^2 T_t(x, y, t) + \rho_b c_b \frac{\omega_b}{e^{\Omega(x, y, t)}} (T_b - T_t(x, y, t)) + Q_m(x, y) + Q_p(x, y) \quad (4)$$

Healthy Tissue:

$$\rho_h c_h \frac{\partial T_h(x, y, t)}{\partial t} = k_h \nabla^2 T_h(x, y, t) + \rho_b c_b \frac{\omega_b}{e^{\Omega(x, y, t)}} (T_b - T_h(x, y, t)) + Q_m(x, y) \quad (5)$$

In Eqn.4 and 5, t denotes time, ρ , c , T , k denote the tumor/tissue density, specific heat of the tumor/tissue, local tumor/tissue temperature and thermal conductivity, respectively. ω_b , ρ_b , c_b , T_b denote blood perfusion rate, blood density, specific heat and temperature of blood, respectively. Q_m and Q_p denote the metabolic heat generation rate in the tumor/tissue and the point heat source due to magnetic nanoparticles. Ω is called tumor/tissue damage [12] and it is defined using Arrhenius equation as:

$$\Omega(x, y, t) = A \int_0^t e^{-E_a/R_u T(x, y, t)} dt \quad (6)$$

In Eqn.6, A , E_a , R_u denote pre-exponential factor, activation energy and universal gas constant, respectively. The Arrhenius equation is a formula for the temperature dependence of reaction rates in chemical fields. The integral over time means the extent of reaction proceeds. Here it is used

to estimate the cumulative damage to tumor/tissue. The term $\frac{1}{e^{\Omega}}$ is a correction factor to the perfusion term considering the decrease in local blood perfusion due to tumor/tissue damage at higher temperatures.

The governing equation is solved implicitly and point-wise by COMSOL.

Fig.8 shows the COMSOL time step.

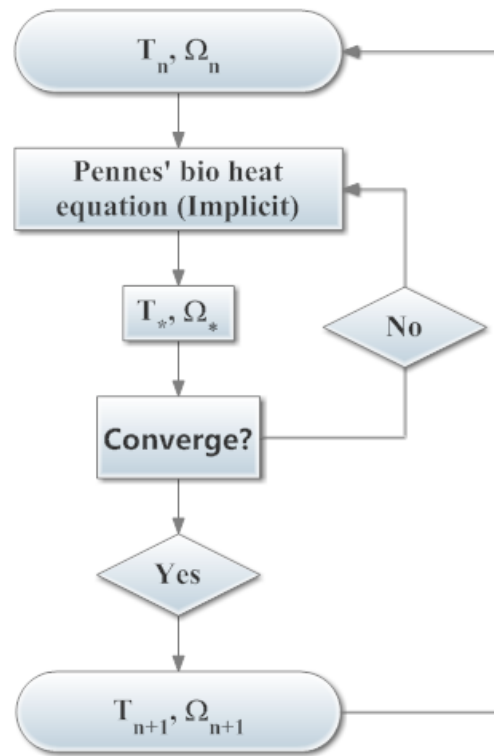


Figure 8 Flow chart of each time step

2.3.4 Boundary and initial conditions

The boundary condition at the interface between the tumor and the normal tissue is the as continuity of temperature and heat flux:

$$k_t \frac{\partial T_t(x,y,t)}{\partial n} = k_h \frac{\partial T_h(x,y,t)}{\partial n} , T_t(x,y,t) = T_h(x,y,t) ; at \frac{x^2}{a_1^2} + \frac{y^2}{b_1^2} = 1 \quad (7)$$

At the tissue boundary, the constant temperature boundary condition

corresponding to core body temperature 37°C:

$$T_h(x, y, t) = 37^\circ\text{C} ; \text{at } \frac{x^2}{a_2^2} + \frac{y^2}{b_2^2} = 1 \quad (8)$$

In Eqn.7 and 8, $a_1= 0.0045\text{m}$, $b_1= 0.003\text{m}$, $a_2= 0.0095\text{m}$ and $b_2=0.008\text{m}$.

The initial temperature is 37°C in both tumor and healthy tissue regions:

$$T(x, y, t = 0) = 37^\circ\text{C} ; \text{at } \frac{x^2}{a_2^2} + \frac{y^2}{b_2^2} \leq 1 \quad (9)$$

2.3.5 Time and mesh configuration

The total time of interest for this study is 1200s. The time step is 1s. The mesh type is normal in COMSOL. Fig.9 shows the finite element meshes of the four models in COMSOL.

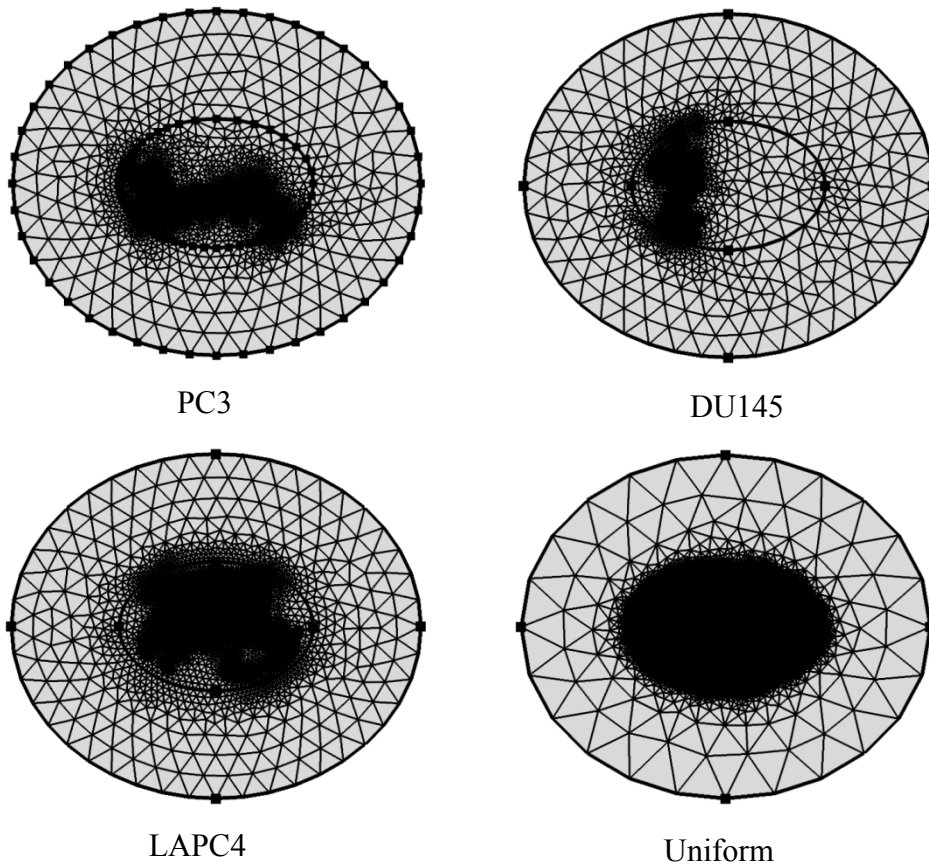


Figure 9 Meshes of the four models in COMSOL

A sensitivity study is carried out to test how the time step and the mesh type we choose would affect the results. The mesh sensitivity study is conducted by comparing the maximum temperatures in the computational domain for different mesh types. The time step remains unchanged at 1s. The time step sensitivity study is carried out by comparing the maximum temperatures for different time steps. The mesh types remain unchanged (normal type). The results are summarized in Table 3 and Table 4. In Table 3, the numbers in the parentheses are numbers of elements in the mesh.

<i>Mesh types</i>	<i>PC3</i>	<i>DUI45</i>	<i>LAPC4</i>	<i>Uniform</i>
<i>Coarser</i>	<i>48.864°C(12562)</i>	<i>52.778°C(11942)</i>	<i>48.123°C(13902)</i>	<i>45.235°C(29308)</i>
<i>Normal</i>	<i>48.864°C(18104)</i>	<i>52.778°C(13714)</i>	<i>48.124°C(19038)</i>	<i>45.235°C(45080)</i>
<i>Extra Fine</i>	<i>48.864°C(24806)</i>	<i>52.781°C(22066)</i>	<i>48.125°C(27932)</i>	<i>45.237°C(57814)</i>

Table 3 Maximum temperature among four models for different mesh types

<i>Time steps</i>	<i>PC3</i>	<i>DUI45</i>	<i>LAPC4</i>	<i>Uniform</i>
<i>0.2s</i>	<i>48.864°C</i>	<i>52.778°C</i>	<i>48.124°C</i>	<i>45.235°C</i>
<i>1s</i>	<i>48.864°C</i>	<i>52.778°C</i>	<i>48.124°C</i>	<i>45.235°C</i>
<i>5s</i>	<i>48.864°C</i>	<i>52.778°C</i>	<i>48.124°C</i>	<i>45.235°C</i>

Table 4 Maximum temperature among four models as a function of time steps

In Table 3 and Table 4, the variations of maximum temperature are less than 0.006% both for mesh and time step variations. The results indicate that the mesh type and the time step we select are appropriate.

3. Results and discussion

The primary interest of this study is to analyze the effect of nanoparticle distribution on hyperthermia treatment. The analysis includes temperature distribution, maximum temperature, time required to reach steady state, CEM43, iso-effective dose and heat flux at tumor-tissue boundary.

3.1 Temperature distribution

The temperature distributions directly provide basic information about the magnetic nanoparticle hyperthermia effect on the tumor and healthy tissue. It is useful for the assessment of treatment protocols. However, the determination of temperature distribution throughout both tumor and healthy tissue is difficult in clinical studies since temperatures are sampled at only a limited number of locations using conventional sensors [8]. In the present study we numerically computed the temperature distributions of the four models. The results are displayed in fig.10. As can be observed in the figure, each of the models exhibits a different temperature distribution and maximum temperature (45.2°C-52.8°C). Locations with higher nanoparticles concentration have higher temperatures.

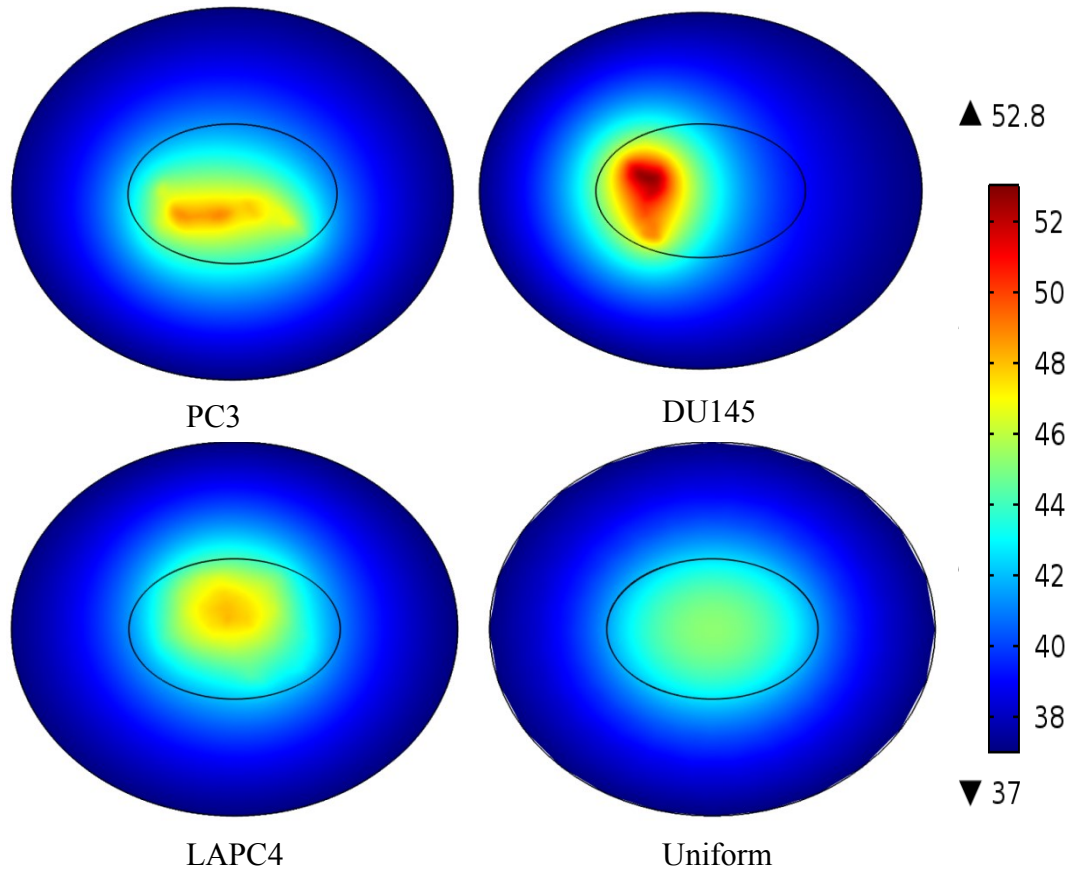


Figure 10 Temperature distribution in tumor and healthy tissue after heating of 1200s for $Q_e=5.51 \times 10^5 \text{W/m}^2$

3.2 Maximum temperature and time to reach steady state

Fig.11 shows the maximum temperature in the computational domain with time. Fig.12 shows the maximum temperatures attained and the time needed to reach steady state in both tumors and tissues. The time to reach steady state t_s is calculated as:

$$\frac{T(t_s)-T_i}{T_f-T_i} = 0.99 \quad (10)$$

where T_i , T_f denote initial and final temperature.

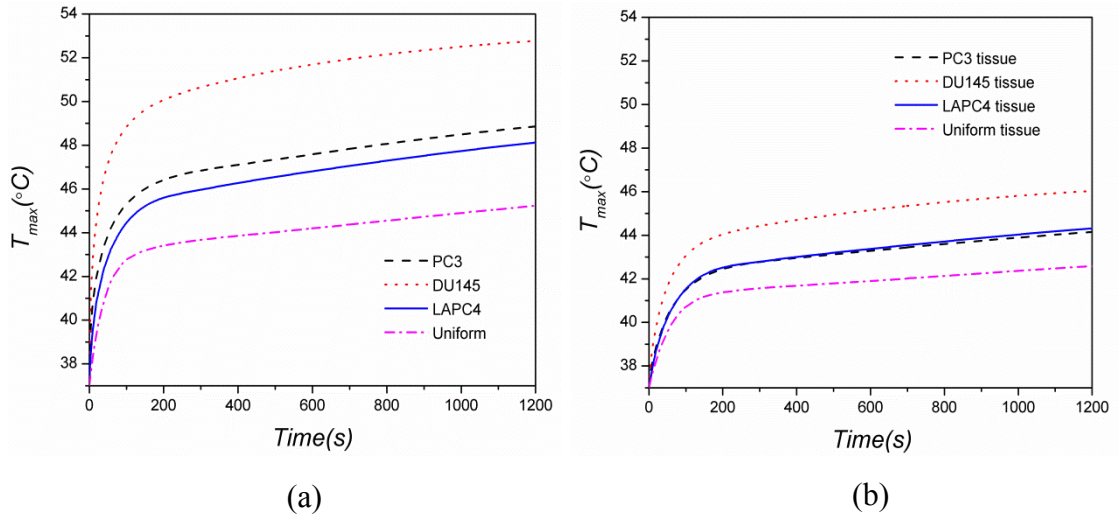


Figure 11 Maximum temperatures in tumor and healthy tissue with time

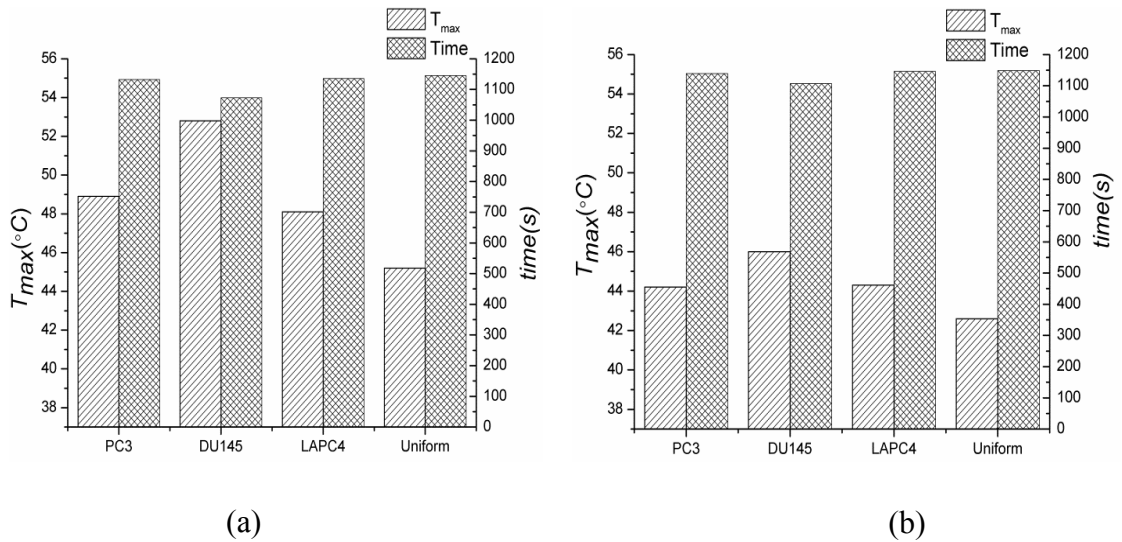


Figure 12 Maximum temperature attained and time needed to reach steady state in (a) tumor and (b) healthy tissue for $Q_e = 5.51 \times 10^5 \text{ W/m}^2$

The order of t_s in both tumors and healthy tissues from small to large is DU145 (1073s, 1107s), PC3 (1132s, 1139s), LAPC4 (1136s, 1146s) and Uniform (1145s, 1149s). It is the same order as that of distributions from concentrated to uniform. It indicates that more concentrated distribution takes less time to reach the steady state. The reason is that in concentrated distribution models, tumors are heated concentrative and the temperature

gradients between the adjacent points in both tumors and healthy tissues are larger than those in uniform distribution models. The diffusion is proportional to temperature gradient. So the heat diffuses faster in a concentrated distribution model.

In terms of the maximum temperatures, DU145 has the highest maximum temperatures (52.8°C, 46°C) in both tumors and healthy tissues, while Uniform has the lowest ones (45.2°C, 42.6°C). PC3 has maximum temperatures 48.9°C, 44.2°C and LAPC4 has maximum temperatures 48.1°C, 44.3°C in tumors and healthy tissues. We can thus conclude that more concentrated nanoparticle distribution would result in higher temperature under the same amount of total heat source in magnetic nanoparticle hyperthermia. A higher temperature in the tumor means more efficiency in treatment, while a higher temperature in the healthy tissue means more undesired damage. However, if the maximum temperature exceeds a certain threshold (45°C), it would cause discomfort. Since the differences of steady state time (within 4.5%) are smaller than those of the maximum temperature (within 16.7%), considering both maximum temperature and steady state time, we can conclude that more concentrated nanoparticle distribution is more efficient in hyperthermia treatment within suitable thermal dose ranges, but it may make patients uncomfortable due to a higher temperature increase in a shorter time. The

results can help physicians to choose the desired heat dose according to nanoparticle distributions and therapy protocols.

3.3 CEM43 contour

The results in sections 3.1 and 3.2 help us understand the effect of magnetic nanoparticle hyperthermia on tumors and tissues. However, criteria that can be used to directly compare the effects of different hyperthermia treatments should be introduced. CEM43 is one of these criteria and it is widely used in clinical studies.

Since the temperatures in a hyperthermia process vary with time and temperatures in different hyperthermia processes change in different rates, it is difficult to evaluate and compare the heating effects in different processes. One solution is to convert the effect of temperature-varying process into that of a constant temperature process. To achieve the same heating effect, the time taken in a constant temperature process, which we call it equivalent time, is different from the original time (fig.13).

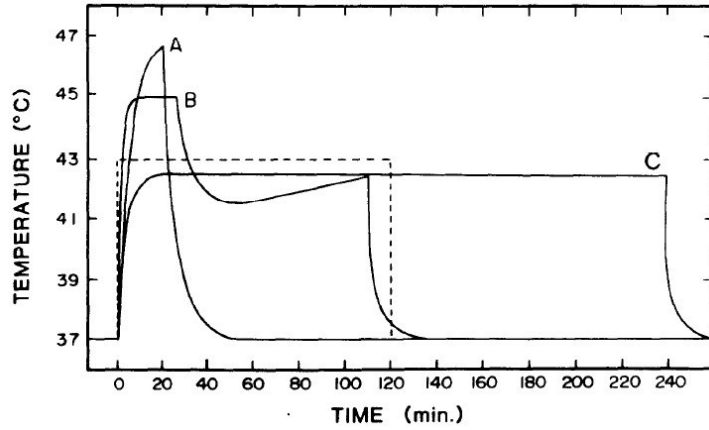


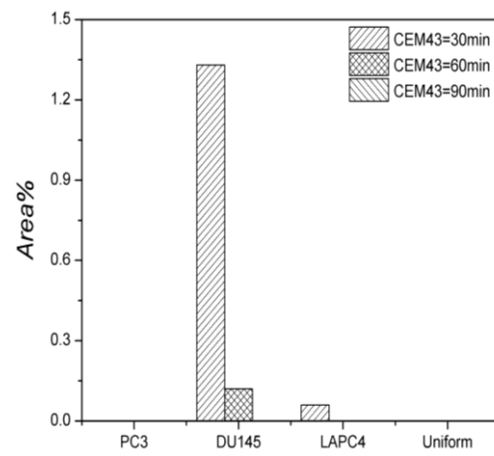
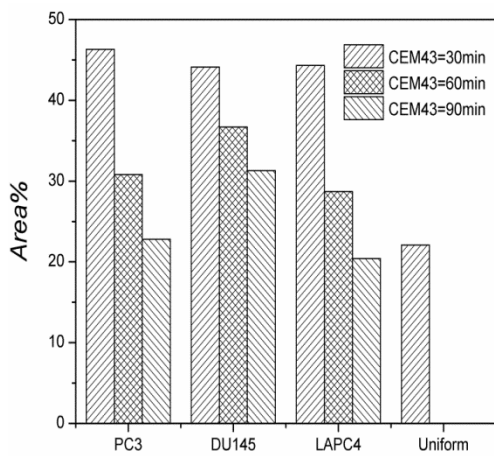
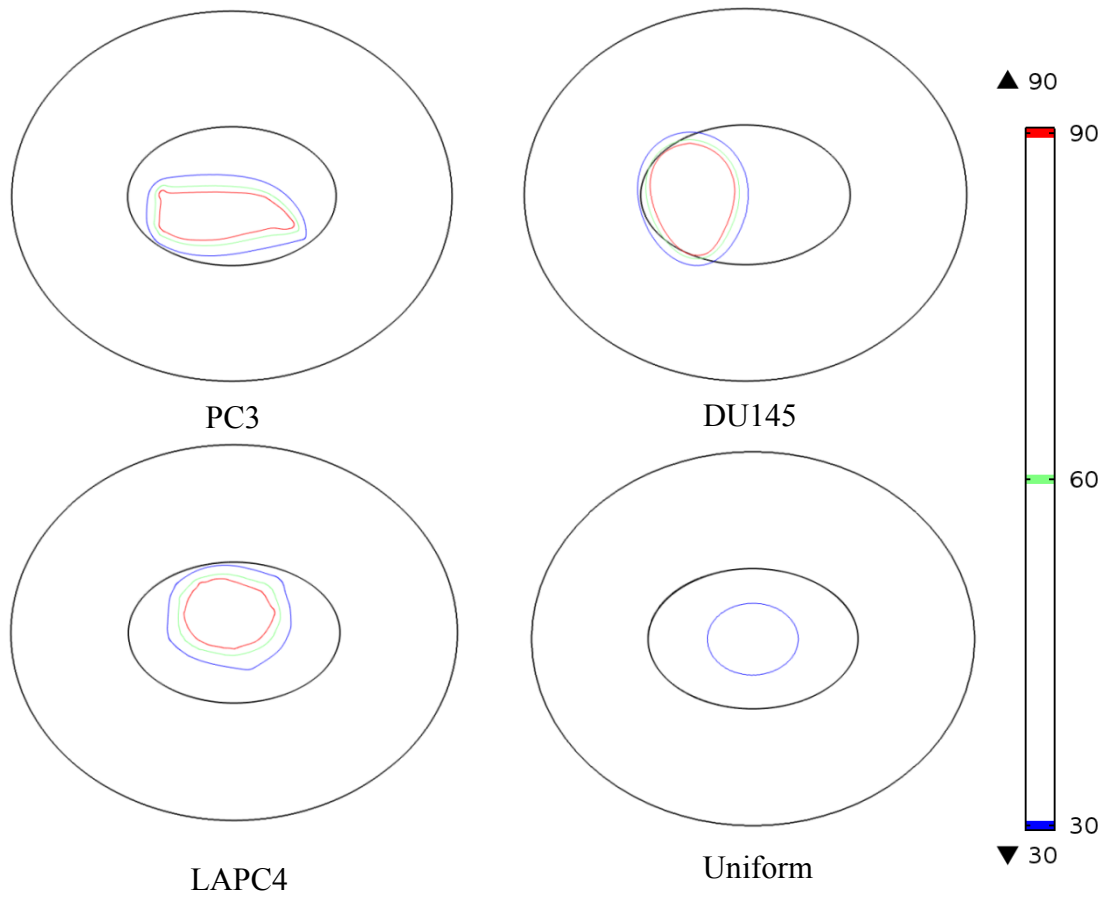
Figure 13 temperature profiles in different hyperthermia processes [17]

The effect of a hyperthermia process then can be evaluated by calculating the equivalent time. CEM43 is cumulative equivalent minutes heating at a constant temperature at 43°C. The expression of CEM43 is as [17]:

$$CEM43(x, y) = \int_0^t R^{43-T(x,y,t)} dt \quad (11)$$

Where $R = 0.5$ for $T > 43^\circ\text{C}$, and $R = 0.25$ for $T < 43^\circ\text{C}$.

The contours of $CEM43=30, 60, 90\text{min}$ for the four models are displayed in fig.14. Fig.15 compares the percentage of tumor and healthy tissue area for $CEM43>30, 60, 90\text{min}$ among the models.



(a)

(b)

Figure 15 Percentage area of (a) tumor and (b) healthy tissue with CEM 43 > 30, 60, 90min for $Q_e = 5.51 \times 10^5 \text{ W/m}^2$

In magnetic nanoparticle hyperthermia, the local point of tumor/tissue whose CEM43 is larger than 60min is considered as having achieved enough heating effect so that it is thermally damaged [18]. For CEM43 > 60min, PC3, DU145, LAPC4 and Uniform have 30.8%, 36.7%, 28.7% and 0% damaged tumor area as well as 0%, 0.1%, 0% and 0% damaged healthy tissue area, respectively. DU145 has the largest damaged tumor area and the largest damaged healthy tissue area. PC3 has a larger damaged tumor area than LAPC4. Uniform model has the smallest damaged tumor area and damaged healthy tissue area. This is expected because in the uniform distribution model, more percentage area of the tumor is covered with nanoparticles leading to more tumor area having a lesser thermal dose. The percentage of tumor area exhibiting high amount of thermal dose is small when compared to all the other three models at the same total heating power.

Since our primary interest is the tumor damage and all the healthy tissue damage area of the four models are less than 0.1%, we can conclude the tissue damage is less significant than the tumor damage. Considering both the tumor and healthy tissue damage, we can conclude that DU145, PC3, LAPC4 and Uniform have the treatment effect from best to worst. The conclusion implies that a more concentrated distribution model has a better effect of destroying diseased tissue at the given heating power.

3.4 Iso-effective dose

Iso-effective dose is the heating power needed to achieve $CEM_{43} > 60\text{min}$ in 90% of the tumor area [16]. Iso-effective doses for each of the models are computed and plotted in fig.16.

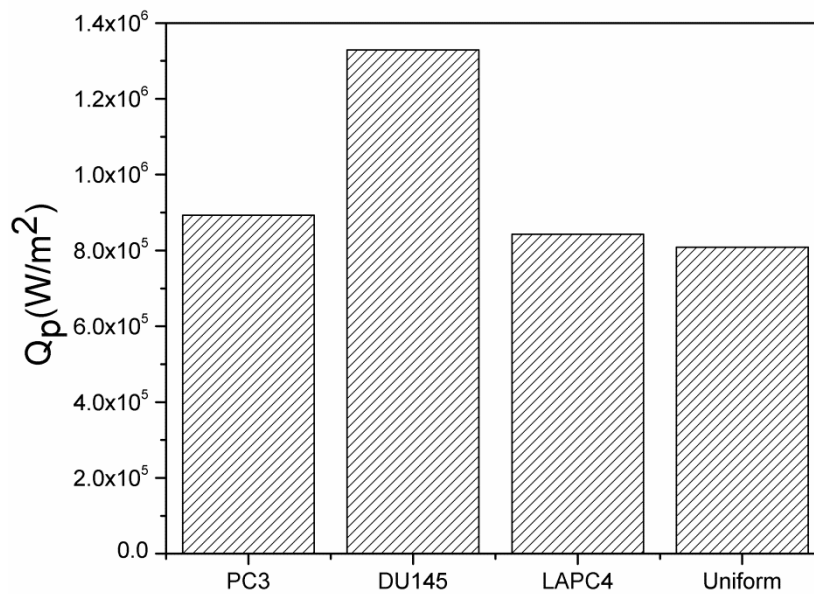


Figure 16 Iso-effective doses for each of the tumor models

It can be observed that DU145 needs the largest thermal dose to achieve $CEM_{43} > 60\text{min}$ in 90% of the tumor area and Uniform requires the smallest thermal dose. The result indicates that uniform distribution has the highest efficiency in treatment, which does not conform to the conclusion we draw in section 3.3. The reason is that at iso-effective dose (which is much larger than $Q_e = 5.51 \times 10^5 \text{ W/m}^2$), although the uniform distribution model still has a lesser thermal dose, this dose now is enough to damage the tumor ($CEM_{43} > 60\text{min}$).

Combining the results of all the previous sections, we can conclude that a more concentrated distribution model has a better treatment effect at low heating powers while at high heating powers uniform distribution model has better effect. However, the maximum temperatures for iso-effective doses are 5-10°C higher than those in $Q_e = 5.51 \times 10^5 \text{ W/m}^2$, it would be less possible for patients to bear with.

Notice that the iso-effective dose of DU145 is significantly higher (64.6%) than those of the other three models. This special feature of DU145 is discussed and explained in section 3.6.

3.5 Heat flux at tumor-tissue boundary

We calculate the heat flux at the tumor-tissue boundary for $Q_p = 5.51 \times 10^5 \text{ W/m}^2$. The result is plotted in fig.17.

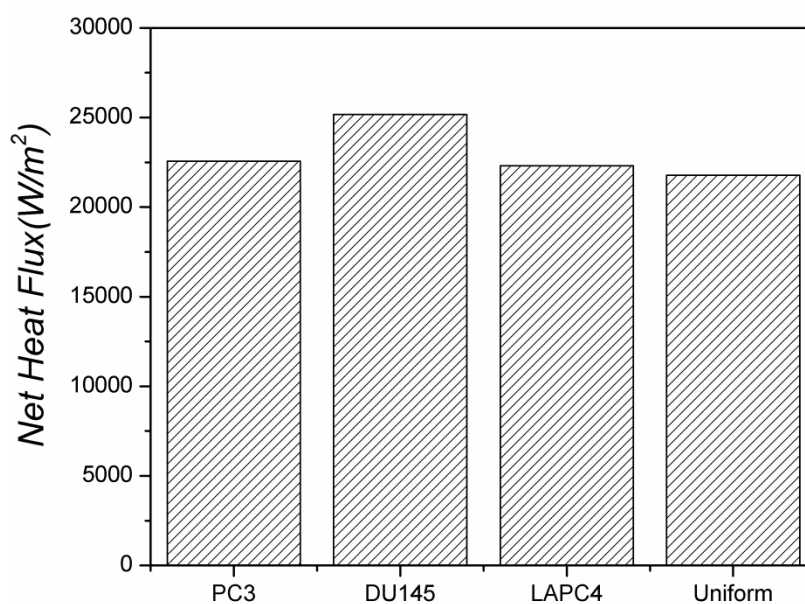


Figure 17 Heat flux at the tumor-tissue interface for $Q_e = 5.51 \times 10^5 \text{ W/m}^2$

It can be seen clearly that DU145 has the most heat flux (25168W/m^2) passing through the tumor-tissue boundary. It needs to be noted that, more heat flux passing the tumor – tissue boundary means more undesired heating of the healthy tissue. The heat flux data explains for the previous result of the percentage of healthy tissue area with CEM $43>30$ and 60min (fig.15b) where DU145 model had the most percentage area of all the four models.

The reason for the large heat flux for DU145 may lie in its nanoparticle distribution—the nanoparticles are concentrated too close to the tumor-tissue boundary (fig. 6b). To verify this, we move the concentrated nanoparticles in DU145 to the center of the tumor and calculate similar results to the previous ones. The new model is named Concentrated model.

3.6 The concentrated model

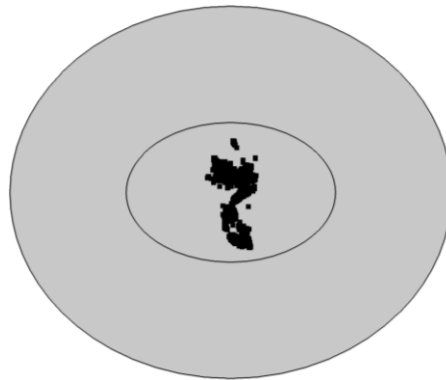


Figure 18 Computational model of the concentrated model with nanoparticles

Temperature distribution

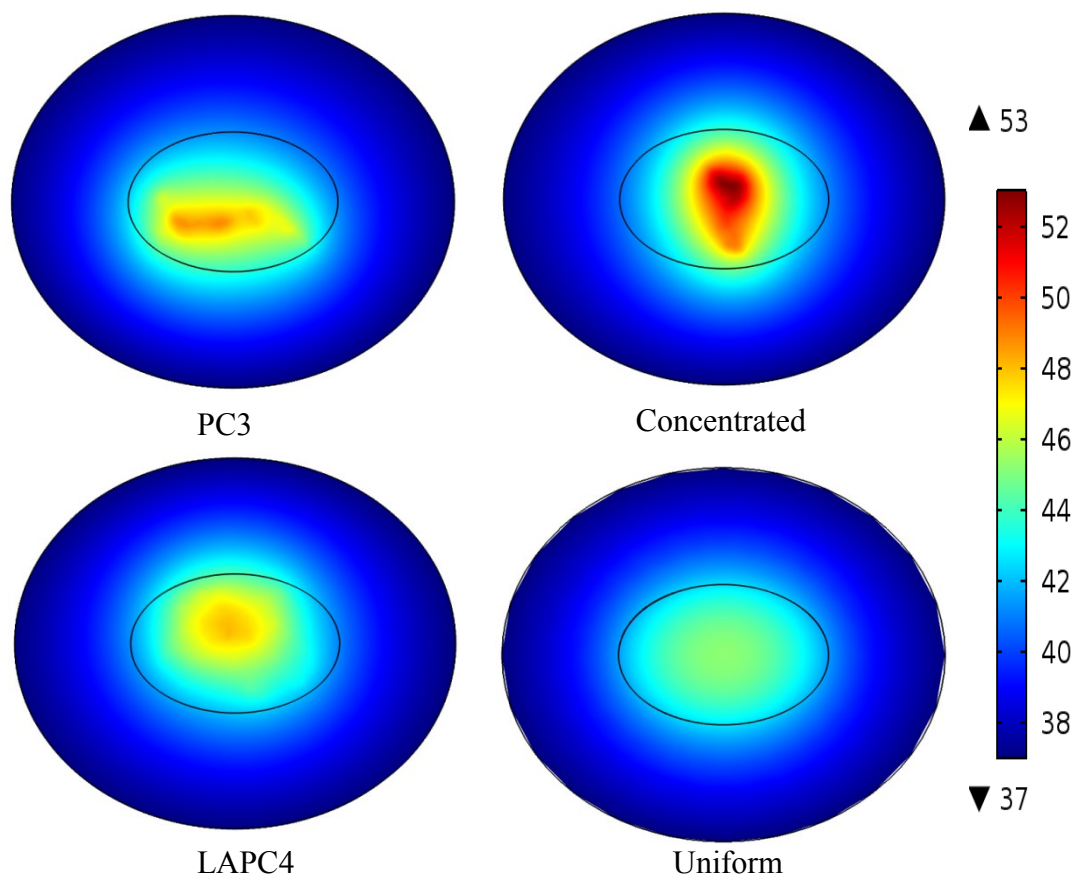


Figure 19 Temperature distributions in tumor and tissue after heating of 1200s for $Q_e = 5.51 \times 10^5 \text{ W/m}^2$

Maximum temperature and time needed to reach steady state

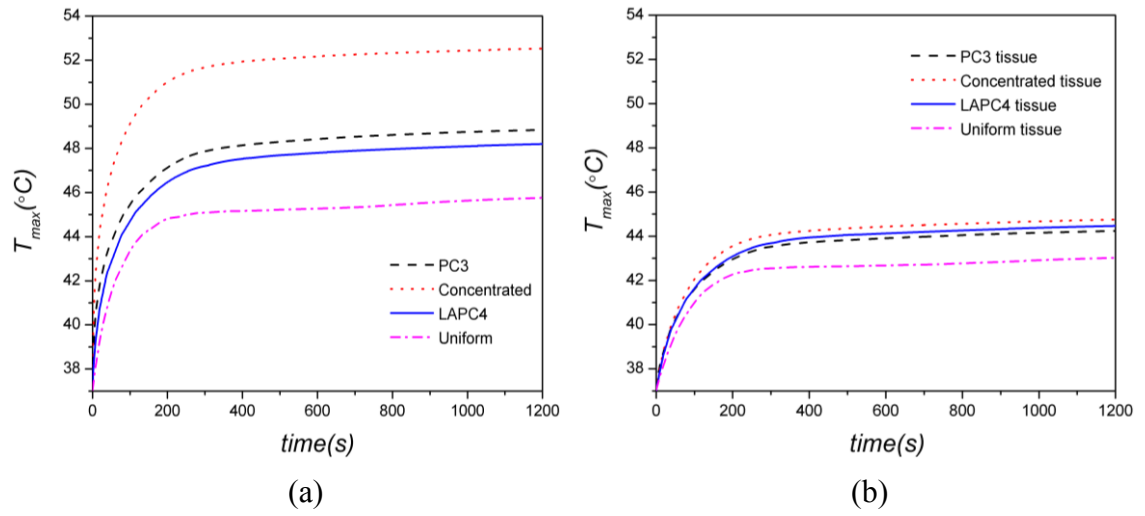


Figure 20 Maximum temperatures in tumor and healthy tissue with time

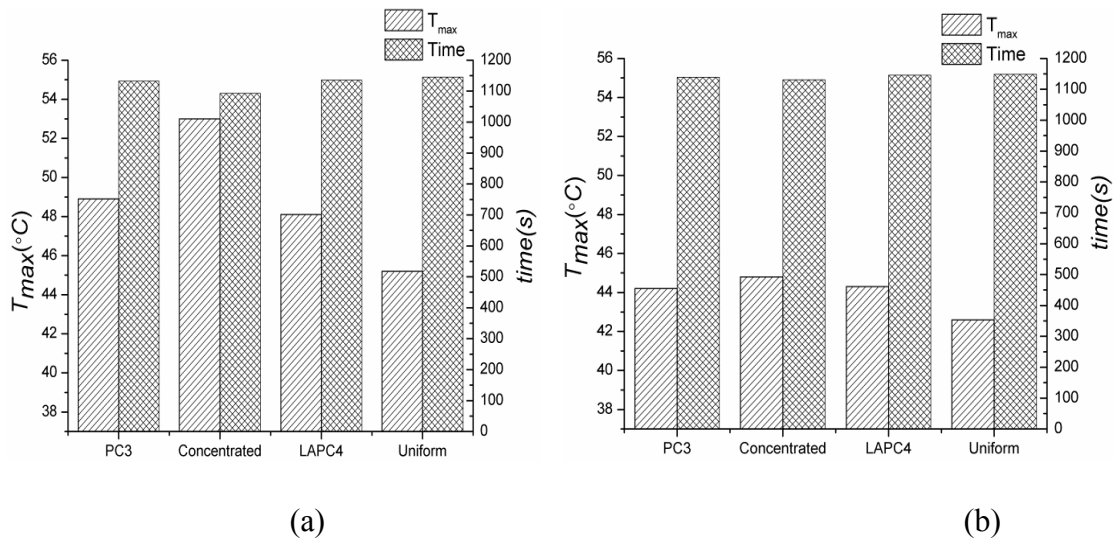


Figure 21 Maximum temperature and time attained at steady state in (a) tumor and (b) healthy tissue for $Q_e = 5.51 \times 10^5 \text{ W/m}^2$

CEM43 contour

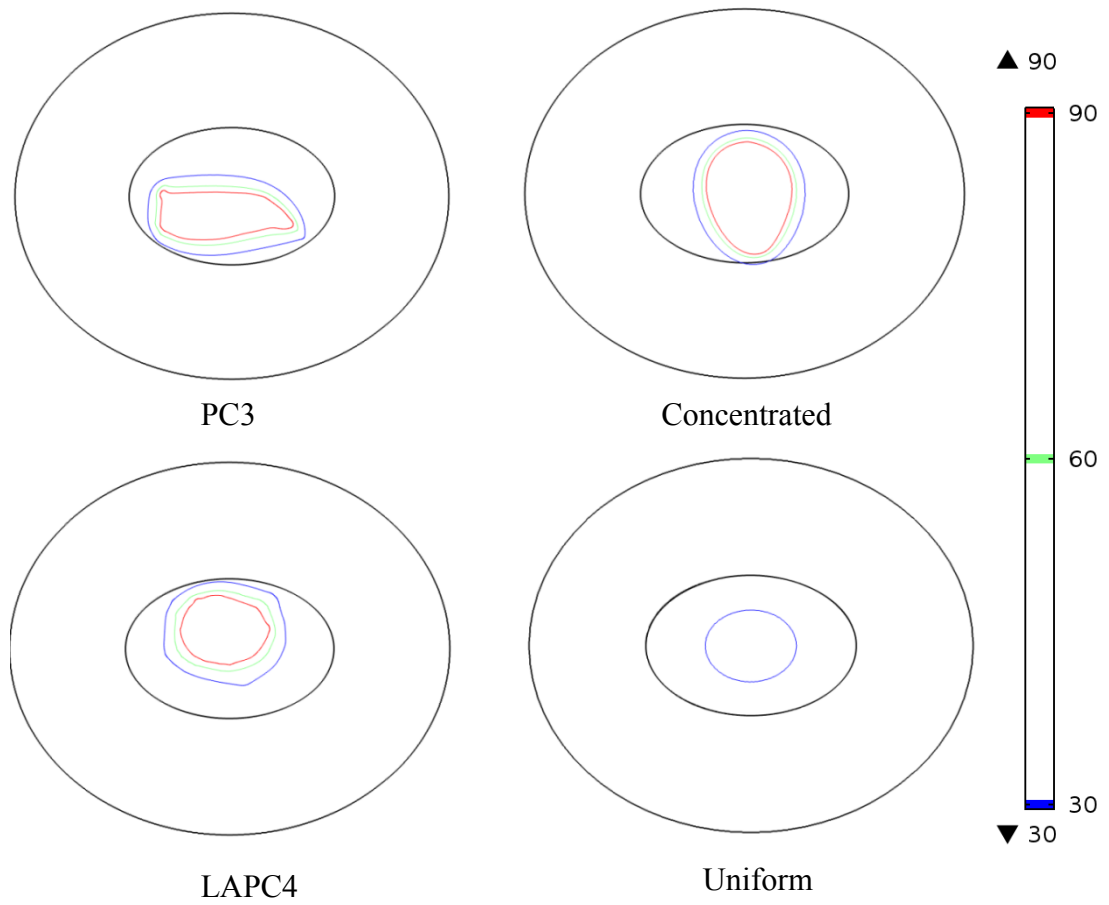


Figure 22 CEM43=30, 60, 90min for $Q_e = 5.51 \times 10^5 \text{ W/m}^2$

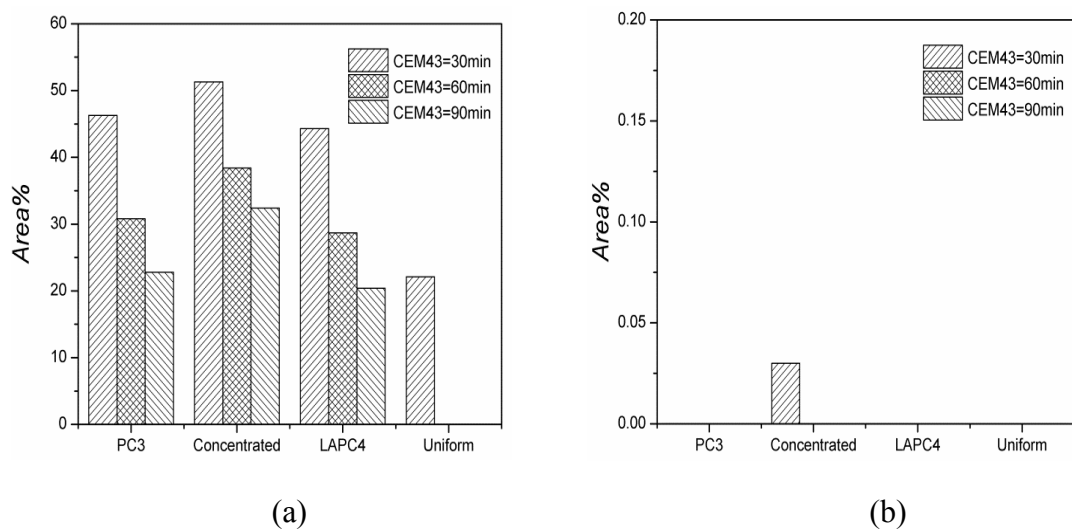


Figure 23 Percentage area of (a) tumor and (b) tissue with CEM 43 > 30, 60, 90min for $Q_e = 5.51 \times 10^5 \text{ W/m}^2$

Iso-effective dose

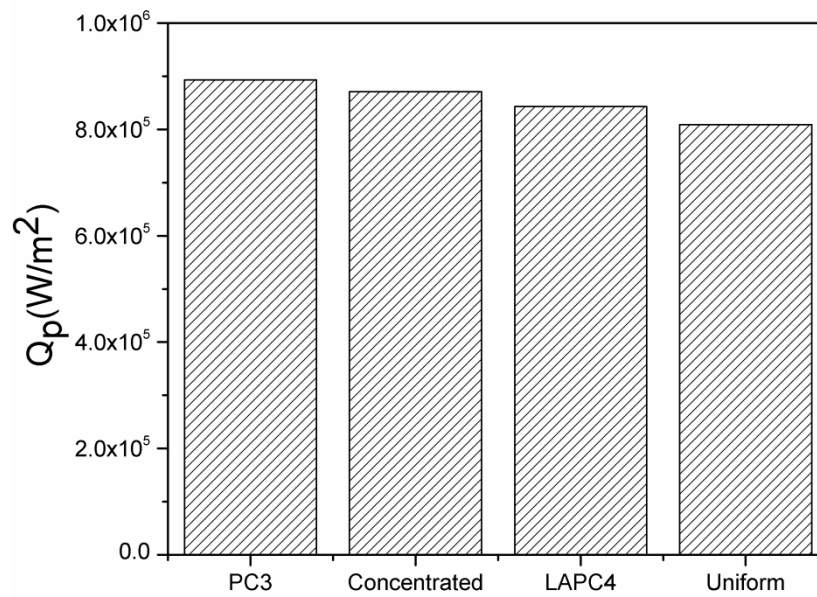


Figure 24 Iso-effective doses for each of the tumor models

Heat flux at the tumor-tissue boundary

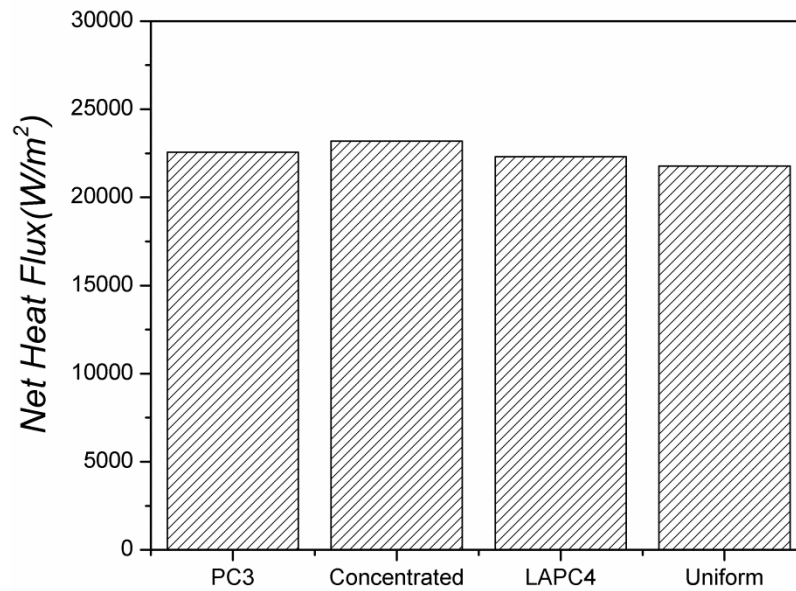


Figure 25 Heat flux at the tumor-tissue interface for $Q_e = 5.51 \times 10^5 W/m^2$

The temperature distribution (fig. 19), the maximum temperature and steady state time (fig. 21) are similar to the previous ones. In fig. 23, the

Concentrated model has the largest percentage of damaged tumor area for CEM43>30, 60 and 90min. For tumor damage (CEM43>60min) at the given heating power, concentrated distribution has a better effect of damaging diseased tissue.

The iso-effective dose of the Concentrated model in fig. 24 and the heat flux in fig. 25 are much smaller than those of DU145 in fig. 16 and fig. 17. The Concentrated distribution has a smaller the iso-effective dose than PC3. It can be concluded that other than the degree of concentration, the location where the nanoparticles are concentrated also affects the treatment effect. The more nanoparticles concentrated near the center of the tumor, the better the effect is. The concentrated model outperforms the uniform one under low heating powers but it is the opposite under high heating powers.

4. Conclusions

This study is based on the images of different nanoparticle distributions in slices of PC3, DU145 and LAPC4 tumors. The color images are processed in MATLAB so that the information regarding nanoparticle distribution and location of nanoparticles is imported into COMSOL models. A uniform distribution model is added as a control group for comparison for an idealized condition. Temperature distribution, maximum temperature, time to reach steady state, CEM43, iso-effective dose and heat flux at tumor-tissue boundary are analyzed to evaluate the effect of the nanoparticle distribution on hyperthermia treatment. The results indicate that a more concentrated nanoparticle distribution has a better effect of damaging diseased tissue than uniform distribution for low heating power. The uniform distribution has better effect than the concentrated distribution for high heating powers. However, it would be less possible for patients to bear with the high temperature (45°C). For concentrated nanoparticle distributions, the location where the nanoparticles are concentrated influences the effect of heating. More centered one has a better effect.

Bibliography

1. Wust P, Hildebrandt B, Sreenivasa G, et al. Hyperthermia in combined treatment of cancer[J]. *The lancet oncology*, 2002, 3(8): 487-497.
2. van der Zee J. Heating the patient: a promising approach?[J]. *Annals of oncology*, 2002, 13(8): 1173-1184.
3. Maeda H, Wu J, Sawa T, et al. Tumor vascular permeability and the EPR effect in macromolecular therapeutics: a review[J]. *Journal of controlled release*, 2000, 65(1): 271-284.
4. Pankhurst Q A, Connolly J, Jones S K, et al. Applications of magnetic nanoparticles in biomedicine[J]. *Journal of physics D: Applied physics*, 2003, 36(13): R167.
5. Gilchrist R K, Medal R, Shorey W D, et al. Selective inductive heating of lymph nodes[J]. *Annals of surgery*, 1957, 146(4): 596.
6. Hergt R, Andra W, d'Ambly C G, et al. Physical limits of hyperthermia using magnetite fine particles[J]. *Magnetics, IEEE Transactions on*, 1998, 34(5): 3745-3754.
7. Moroz P, Jones S K, Winter J, et al. Targeting liver tumors with hyperthermia: ferromagnetic embolization in a rabbit liver tumor model[J]. *Journal of surgical oncology*, 2001, 78(1): 22-29.
8. Strohschein J W, Roemer R B. A survey of computer simulations of hyperthermia treatments[J]. *Biomedical Engineering, IEEE Transactions on*, 1984 (1): 136-149.
9. Halac S, Roemer R B, Oleson J R, et al. Uniform regional heating of the lower trunk: Numerical evaluation of tumor temperature distributions[J]. *International Journal of Radiation Oncology* Biology* Physics*, 1983, 9(12): 1833-1840.
10. Matloubieh A Y, Roemer R B, Cetas T C. Numerical simulation of magnetic induction heating of tumors with ferromagnetic seed implants[J]. *Biomedical Engineering, IEEE Transactions on*, 1984 (2): 227-234.
11. Zhao Q, Wang L, Cheng R, et al. Magnetic nanoparticle-based hyperthermia for head & neck cancer in mouse models[J]. *Theranostics*, 2012, 2(1): 113.
12. Chang I A, Nguyen U D. Thermal modeling of lesion growth with radiofrequency ablation devices[J]. *Biomedical engineering online*, 2004, 3(1): 27.
13. Rylander M N, Feng Y, Stafford R J, et al. Optimizing heat shock protein expression induced by prostate cancer laser therapy through predictive computational models[J]. *Journal of biomedical optics*, 2006, 11(4): 041113-041113-16.
14. McIntosh R L, Anderson V. A comprehensive tissue properties database provided for the thermal assessment of a human at rest[J]. *Biophysical Reviews and Letters*, 2010, 5(03): 129-151.
15. Xu L X, Zhu L, Holmes K R. Thermoregulation in the canine prostate during transurethral microwave hyperthermia, part II: blood flow response[J]. *International journal of hyperthermia*, 1998, 14(1): 65-73.
16. Johannsen M, Gneveckow U, Thiesen B, et al. Thermotherapy of prostate cancer

- using magnetic nanoparticles: feasibility, imaging, and three-dimensional temperature distribution[J]. *European urology*, 2007, 52(6): 1653-1662.
17. Sapareto S A, Dewey W C. Thermal dose determination in cancer therapy[J]. *International Journal of Radiation Oncology* Biology* Physics*, 1984, 10(6): 787-800.
 18. Overgaard J, Bentzen S M, Overgaard J, et al. Randomised trial of hyperthermia as adjuvant to radiotherapy for recurrent or metastatic malignant melanoma[J]. *The Lancet*, 1995, 345(8949): 540-543.
 19. Bordelon D E, Cornejo C, Grüttner C, et al. Magnetic nanoparticle heating efficiency reveals magneto-structural differences when characterized with wide ranging and high amplitude alternating magnetic fields[J]. *Journal of Applied Physics*, 2011, 109(12): 124904.

Curriculum Vitae

Basic Information

Name: Jianan Wang

Gender: Male

Date of Birth: March 24th, 1990

Place of Birth: Hangzhou, Zhejiang Province, China

Education

Johns Hopkins University, Baltimore, MD

Master of Science in Mechanical Engineering (thesis-based)

May 2014

Tsinghua University, Beijing, China

Bachelor of Science in Thermal Engineering

July 2012

Research Experience

Simulation of Magnetic Nanoparticle Hyperthermia in Prostate Tumor (Master's Thesis)

Johns Hopkins University, Baltimore, MD

September 2013 – Present

- Processed images of nanoparticle distributions in prostate tumor using MATLAB.
- Built 2D models and simulated using COMSOL.
- Investigated clinical parameters to help improving cancer treatment protocol.

Experimental Study of Cu-based Oxygen Carrier in Chemical Looping Combustion (Senior Design)

Tsinghua University, Beijing, China

January 2012 – June 2012

- Supported copper oxide with cement to reduce agglomeration.
- Investigated the oxygen carrier multi-cycle reactivity in fluidized bed.

Publications

Xu, L., **Wang, J.**, Li, Z., & Cai, N. (2013). Experimental study of cement-supported CuO oxygen carriers in chemical looping with oxygen uncoupling (CLOU). *Energy & Fuels*, 27(3), 1522-1530.